SUPPLEMENTARY MATERIALS

Concussion, Microvascular Injury, and Early Phosphorylated Tauopathy in Young Athletes after Impact Head Injury and an Impact Concussion Mouse Model

Chad A. Tagge,* Andrew M. Fisher,* Olga V. Minaeva,* *et al.*

*Authors CAT, AMF, OM contributed equally. Correspondence: Lee E. Goldstein, M.D., Ph.D., Boston University School of Medicine, 670 Albany Street, Boston, MA 02118, USA. Email: lgold@bu.edu.

I. CONTENTS — SUPPLEMENTARY MATERIALS

Additional supplementary materials not included in this document:

Supplementary Video 1 Acute neurobehavioral responses in *unanesthetized* C57BL/6 male mice to left-lateral closed-head impact injury or blast exposure at three time points: (i) *before* impact injury or blast exposure, (ii) *immediately after* impact injury or blast

exposure, (iii) *after* 3-hour recovery following impact injury or blast exposure. Representative impact-injured mice: P-199, L-070, P-238. Representative blast-exposed mouse: L-082.

Note 1: Impact injury and blast exposure models produce comparable head kinematics (Supplementary Table 2). **Note 2**: *Experimental impact injury and blast exposure were conducted without anaesthesia to facilitate post-injury neurobehavioral assessment.* See text for details.

Supplementary Video 2 Computational simulation time histories of intracranial shear (von Mises) stress in response to unilateral closed-head impact injury or blast exposure under experimental conditions that produce comparable head kinematics.

II. SUPPLEMENTARY MATERIALS AND METHODS

$CCR2^{RFP}/CX3CR1^{GFP}$ mice

$CCR2^{RFP}/CX3CR1^{GFP}$ male mice (The Jackson Laboratory, Bar Harbor, ME), 10 to 12 weeks-of-age, were group-housed at the Laboratory Animal Science Center, Boston University School of Medicine. Cohort size was 8 to 10 per group or as otherwise noted. $CCR2^{RFP}/CX3CR1^{GFP}$ mice were generated by crossing B6.129(Cg)-Ccr2tm2.1Ifc/J mice that bear RFP-labeled CCR2-expressing peripheral inflammatory monocytes ($CCR2^{RFP}$ mice) with B6.129P-Cx3cr1tm1Litt/J mice that express enhanced green fluorescent protein GFP-labeled fractalkine receptor CX3CR1-expressing, brain-resident microglia ($CX3CR1^{GFP}$ mice). The resulting F1 progeny ($CCR2^{RFP}/CX3CR1^{GFP}$) express both RFP-labeled, CCR2-expressing peripheral monocytes and GFP-labeled, CX3CR1-expressing, brain-resident microglia. Mice were provided with standard mouse chow and water *ad libitum*. Ambient temperature was controlled at 20-22 ºC with 12-hour light-dark cycles. Animal housing and experiments were conducted in accordance with guidelines from the Association for Assessment and Accreditation of Laboratory Animal Care and National Research Council Guide for the Care and Use of Laboratory Animals. All experiments involving mice adhered to provisions in the Animal Welfare Act and were approved by Institutional Animal Care and Use Committees (IACUC) at Boston University School of Medicine.

Human neuropathological analyses

Neuropathological analysis followed established protocols at the Boston University Alzheimer's Disease Center and Chronic Traumatic Encephalopathy Center and included comprehensive examination for all neuro-degenerative conditions (Vonsattel *et al.*, 1995; McKee *et al.*, 2013; McKee *et al.*, 2016). Control sections were

stained without primary antibodies and did not demonstrate detectable signal. Immunofluorescence imaging was conducted with a Zeiss 880 Airyscan confocal microscope with a 10X objective using the Airyscan fast setting. Exposure and gain settings were determined using the field with the highest intensity fluorescence. All subsequent images were taken with the same settings. Resolution was determined using 2x Nyquist sampling followed by Airyscan processing (deconvolution).

Murine neuropathological analyses

Mice were euthanized by CO_2 asphyxiation according to an IACUC-approved protocol and transcardially perfused with phosphate-buffered saline (PBS, Sigma-Aldrich, St Louis, MO, USA). Brains were rapidly removed from the calvarium and placed in 10% neutral buffered formalin for 2 hours, then transferred to PBS. Coronal slabs (2 mm) were obtained by block sectioning, fixed in 4% paraformaldehyde for 2 hours, embedded in a single paraffin block, and serially sectioned at 10 μm. Sections were processed for immunohistochemistry with a battery of primary antibodies (see Methods) and visualized by Vectastain Elite ABC Kit (Vector Laboratories, Burlingame, CA, USA). Slides were developed according to manufacturer's instructions for exactly the same incubation time and counterstained with hematoxylin. For double immunostained sections, tissue was blocked with avidin and biotin before primary antibody incubation and visualized with diaminobenzidine and aminoethylcarbazole according to the manufacturer's instructions (Vector Laboratories). Murine neuropathology for the one-impact exposure experiment was conducted as follows. Sections of paraffin embedded tissue were cut 20μm thick and fixed to slides. The tissue was stained using a Bond RX (Leica, Buffalo Grove, IL) tissue stainer. Tissue sections were deparaffinized using Bond Dewax Solution (Leica, Cat# AR9222). Antigen retrieval was performed at 100ºC for 20 min using ER1 or ER2 (Leica, Cat# AR9961, Cat# AR9640). Peroxidase block was applied (Refine Kit, Leica, Cat#DS9800) for 10 min., followed by 3X rinse with IHC wash buffer (Leica, Cat# AR9590). The following primary antibodies were applied for 1 hour at room temperature: purified mouse anti-neurofilament-H (SMI-34, 835503, Biolegend, San Diego, CA, 1:5000), mouse anti-glial fibrillary acidic protein (GA5, MAB360, Millipore, Billerica, MA, 1:2000), rabbit anti Iba-1 (019-19741, Wako, Cambridge, MA, 1:500), anti-amyloid precursor protein (AB5352, Millipore, Billerica, MA, 1:5000), mouse anti-amyloid-β peptide aa17-24 (4G8, 800703, Biolegend, San Diego, CA, 1:100,000), mouse

anti-phosphorylated tau protein pS202 (CP-13, pS202; Peter Davies Laboratory, Manhasset, NY, 1:200). Sections were washed 3X with IHC wash buffer. Post-primary block was applied (Refine Kit) to the slides, and incubated for 30 min. Slides were then washed 3X with wash buffer. NovoLink Polymer (Refine Kit) was added to the slides and incubated for 30 min. Slides were washed 3X with wash buffer. Chromogen substrate (Refine Kit) was added and developed for 10 min. Slides were washed with dH2O 5X at room temperature. The slides were counterstained with hematoxylin (Refine Kit) for 8 min at room temperature. Fluorescence staining was performed with the Perkin Elmer Opal kit using the manufacturers recommended protocol for the Bond RX tissue stainer with ER2 epitope retrieval. The primary antibody for fluorescent staining was rabbit anti-human IgG (A0423, Dako, Santa Clara CA, 1:100). Immunofluorescence staining of mouse brain sections using *cis*-p-tau and *trans*-p-tau monoclonal antibodies was conducted as previously described (Kondo *et al.*, 2015). Briefly, after treatment with 0.3 % hydrogen peroxide, slides were briefly boiled in 10 mM sodium citrate, pH 6.0, for antigen enhancement. The sections were incubated with primary antibodies overnight at 4°C. The sections were also incubated with Alexa Fluor 488- or Alexa Fluor 568-conjugated, isotype-specific secondary antibodies (Jackson ImmunoResearch, West Grove, PA, USA) for 1 h at room temperature. Blocking buffer (Invitrogen, Carlsbad, CA, USA) was used for each reaction. Sections were washed 4 times with Tris-buffered saline after each step. Labeled sections were visualized with a Zeiss confocal microscope. The gain of confocal laser was set such that no fluorescence signal was detected in sections without primary antibody.

Electron microscopy

Small pieces (1-2 mm cubes) of harvested brain were fixed in 2.5% glutaraldehyde with 2.5% paraformaldehyde in 0.1M sodium cacodylate buffer (pH 7.4) overnight at room temperature, washed in 0.1M cacodylate buffer, post-fixed with 1% osmium tetroxide (OsO_4) with 1.5% potassium ferrocyanide ($KFeCN_6$) for 1 hour, then washed in water. The specimens were then incubated in 1% aqueous uranyl acetate for 1hour, washed, and sequentially dehydrated in increasing grades of alcohol (10 min each in 50%, 70%, 90%, 100%, 100%). Samples were treated in propylene oxide for 1 hour, infiltrated overnight in a 1:1 mixture of propylene oxide and TAAB Epon (Marivac Canada Inc., St. Laurent, Canada), and polymerized at 60°C for 48 hours. Ultrathin sections (60 nm) were cut on a Reichert Ultracut-S microtome, placed on copper grids, stained with

lead citrate or uranyl acetate, and examined using a Tecnai-G2 Spirit BioTWIN electron microscope. Images were acquired with an AMT 2K CCD camera.

Impact instrument design and operation

A custom computer control program was used to trigger release of high-pressure gas into the instrument barrel. The released gas initiated sudden acceleration of a stainless steel slug of known mass in the instrument barrel. Vent holes at the distal end of the barrel released gas behind the slug such that constant velocity was attained prior to momentum transfer. Terminal slug velocity (pre-impact) was measured for every shot by monitoring light gate interruptions. Slug momentum was transferred to a captive impact rod (constrained by high-performance ceramic bearings) that transferred momentum again by contacting a stainless steel plate on a movable sled that was constrained to linear translation by a low-friction monorail track. Traumatic head motion was initiated by a final momentum transfer mediated by a padded metal plate that was fixed to the mobile sled. A foam pad (ISODAMP® C-1000 Series, EAR Specialty Composites, Indianapolis, IN) was permanently attached to the inner surface of the metal plate. Unanesthetized mice were positioned in the device such that the left-lateral surface of the head was in contact with the foam pad. Linear translation of the sled resulted in acceleration of the head in the horizontal plane of motion (Fig. 2A, B). Slug and rod velocities were measured for each impact by light gates. Sled velocity was determined with a laser displacement sensor (optoNCDT 1630-20, Micro-Epsilon USA, Raleigh, NC) operated at 100 kHz. Instrument data were acquired and processed in MatLab (MathWorks, Natick, MA). The instrument demonstrated accurate, reproducible, and reliable performance within the range of fire pressures used in the animal experiments (Supplementary Table 2A). Performance analysis confirmed repeatable, linearly increasing rod and sled velocities across a range of fill pressures (9.7, 19.6, 30.0, 39.9 psig). Rod velocities ranged between 5.3 m/s and 10.4 m/s (R^2 = 0.98; RSD, 0.6% to 1.6%). Sled velocities ranged between 3.9 m/s to 7.4 m/s (R^2 = 0.97; RSD 7.6% and 9.3%).

Closed-head impact injury mouse model

Unanesthetized mice were pretreated with analgesic (buprenorphine, 0.2 mg/kg, intraperitoneally), placed in a modified DecapiCone (Braintree Scientific, Inc., Braintree, MA), and secured in the prone position such that the

head and cervical spine extended beyond the restraint and the left temporal-zygomatic region of the head was in contact with the inner pad of the impactor. The head and cervical spine were unrestrained. A Velcro strap was used to secure the torso while allowing unrestrained mobility of the cervical spine and head during experimental injury exposure. Mice were exposed to either (i) single impact or (ii) two impacts separated by 15 minutes (single repeat). The single-repeat design represents a minimal condition for repetitive closed-head impact injury as commonly occurs during a session of contact sport play or practice (Broglio *et al.*, 2009; Daniel *et al.*, 2012; Baugh *et al.*, 2015). Experimental closed-head impact injury produced by this mouse model (single, single-repeat) is results in 100% survival (0% mortality) without skull fracture, hemorrhage (subdural, epidural, subarachnoid, superficial laceration), cervical trauma, spinal cord injury, or post-traumatic apnea.

High-speed videography and kinematic analysis

High-speed videography was conducted with a FASTCAM SA5 camera (Photron USA, Inc., Tech Imaging, Saugus, MA) operated at 10 μs frame capture rate (100 kHz) as previously reported (Goldstein *et al.*, 2012). Videographic records were reassembled with ImageJ software and processed in MatLab (MathWorks, Natick, MA). A 2 kHz, second-order, zero-phase Butterworth filter was applied to position versus time data. First, second, and third derivatives (i.e., velocity, acceleration, jerk, respectively) were calculated from filtered position *versus* time vectors using discrete differentiation. To calculate swing radius, head position coordinates were extracted from the top-down camera and fitted by circular regression (Taubin, 1991; Chernov, 2010).

Acute neurobehavioral response test battery

Objective assessment of transient neurobehavioral responses following experimental closed-head impact injury, blast exposure, or sham (no-injury) control conditions was conducted in awake, non-anesthetized (anesthesia-naïve) C57BL6 male mice. The test battery comprised three subtests: open field exploration, inverted mesh navigation, and beam walk. Each subtest elicited a spectrum of neurobehavioral deficits that span multiple domains: arousal, responsivity to environmental stimuli, orienting responses, locomotion and exploration, gait and balance, neuromotor function, and habituation. Open field test arena: 38 cm x 56 cm x 11.5 cm (width x length x wall height) plexiglass box. Inverted wire mesh: 0.5 in (1.27 cm) stainless steel mesh (hardware cloth)

cut to a 42 cm square. Black markings outlined a central 20 cm square on the wire mesh. Beam walk: 1 cm x 100 cm (width x length) plastic beam placed 16 cm above a table. Each subtest was evaluated for 30 seconds. For the open field test, individual mice were placed in the center of the arena and allowed to freely explore the arena for 30 seconds. For the inverted wire mesh test, mice were placed in the center of the wire mesh that was then inverted 180° so that the mouse grasps the wire struts and hangs underneath the inverted mesh. Testing for 30 seconds began once the wire mesh was in the horizontal inverted position. A central box was marked on the inverted side of the wire mesh to allow an observer to score performance. The inverted wire mesh was held directly above the center of the open field arena for 30 seconds. Following the inverted mesh subtest, the mouse was transferred to the center of a 1 cm wide x 100 cm long plastic beam that was elevated 16 cm above a support table. Each beam walk test was conducted for 30 seconds. Neurobehavioral performance on each subtest was graded by a trained observer according to a six-point scale (0–5) based on standardized metrics that capture graduated neurobehavioral impairments specific for each test (Supplementary Fig. 1B). A composite score for the acute neurobehavioral response test battery was calculated based on the combined scores of each of the three subtests. A composite score of 15 indicated unimpaired performance in all three subtests. Lower composite scores correspond to increasing post-injury neurobehavioral impairment (mild: 14–10; moderate: 9–5; severe: 4–0). Rare post-traumatic seizure was scored 0. The complete test battery (all three subtests) was conducted before injury (baseline), two minutes after impact (post-injury), and 3 hours after injury (recovery). See Supplementary Fig. 1B for details.

Dynamic contrast-enhanced magnetic resonance imaging

Dynamic contrast-enhanced magnetic resonance imaging (DCE-MRI) was performed using 11.7T MRI (Bruker, Ettlingen, Germany) at the Boston University High-Field NMR Imaging Core. Images were acquired using T1-weighted sequence (T1W: axial multi-slice multi-echo, TR/TE = 450/9 ms; in-plane resolution, 0.10 x 0.10 mm; slice thickness, 1 mm; acquisition matrix size: 220 x 220, 16 averages). DCE-MRI images were acquired using T1W gradient echo (fast low angle shot sequence, FLASH: TR/TE = 102/1.9 ms; flip angle, 20˚; in-plane resolution, 0.17 x 0.17 mm; slice thickness, 1.0 mm; acquisition matrix: 128 x 128, scan interval: 13 sec, 150 repetitions). Five pre-injection baseline scans were acquired before dynamic imaging. During the dynamic

sequence, 0.1 ml gadofosveset trisodium (Lantheus Medical Imaging, Inc., North Billerica, MA), 0.25 mmol/ml, was administered by intravenous tail vein injection *via* indwelling catheter inserted prior to imaging. After injection, 145 post-injection scans were acquired over 31 minutes. DCE-MRI imaging data was acquired at the designated time points after impact injury (N = 3 mice). Age-matched naïve mice served as controls (N = 3 mice). Post-acquisition image analysis was performed as previously reported (Chassidim *et al.*, 2013; Weissberg *et al.*, 2014) using customized MatLab scripts (MathWorks, Natick, MA). Briefly, a linear curve was used to fit the time-series of each voxel: $s(t) = A \cdot t + B$, where s(t) is the fitted signal. A, the permeability index (in units of intensity/time), is defined by linear fit slope and reflects contrast agent accumulation in the brain. This metric represents a quantitative index of focal blood-brain barrier permeability at a given imaging locus.

Flow cytometry immunophenotyping

Myeloid cells in the brain were isolated from impact-injured and control mice and immunophenotyped by flow cytometry as previously reported (Jay *et al.*, 2015). Mice were sacrificed and perfused by gravity-driven transcardial perfusion with PBS. Harvested whole brains were minced and digested in papain (Roche) at 37°C with shaking for 30 min. Homogenates were passed through 18G and 22G needles, then transferred into 20% FBS. Isotonic Percoll was added to create a 30% solution, underlaid with 1 ml of 70% Percoll, and centrifuged at 800 *g* for 30 min. After centrifugation, 2–3 ml of the 70%–30% interface was collected and washed. Samples were resuspended in FACS buffer (PBS, 1% BSA, 0.1% NaN_3, 5 mM EDTA) and blocked with a CD16/CD32 antibody (1:200; BD, Franklin Lakes, NJ) for 10 min. Pooled sample portions were used for unstained and single-stained control, whereas individual samples were stained with a master mix of CD45/AX700 (1:500; BioLegend, San Diego, CA), CD11b/BV605 (1:500; BioLegend), F4/80/PEefluor610 (1:125; eBioscience, ThermoFisher Scientific, Waltham, MA), and Ly6C/PECy7 (1:50,000; BioLegend). Each sample was divided in two tubes, a fluorescence minus one "FMO" control and an "ALL" sample to which TREM2/APC (1:125; R&D Systems, Minneapolis, MN) was added. Events were acquired on a Fortessa SORP (BD) and analyzed using FlowJo (FlowJo, LLC, Ashland, OR). For analysis, events were gated on single cells and CD11b-positive events. Samples with >5,000 $CD11b^+$ events were used for analysis. This population was divided into $CD45^{lo}$ and $CD45^{hi}$ subsets. $TREM2^+$ events were assessed by overlaying FMO and ALL plots for each sample and

gating on the population present only in the ALL sample. Significant differences between ages and genotypes were determined using one-way ANOVA and *post hoc* Bonferroni-corrected Student's t tests.

Hippocampal and medial prefrontal cortical electrophysiology

For measurement of axonal conduction velocity in the hippocampus (Supplementary Fig. 4A), two extracellular recording electrodes were placed in hippocampus CA1 *stratum alveus* approximately 200 μm apart and a bipolar stimulating electrode was placed 100 μm from the nearest of the two recording electrodes. The bipolar electrode was used to antidromically activate CA1 pyramidal neuron axons in the *stratum alveus*. The latency differences of the peak negativity between the two recording electrodes and the spatial distance were used to calculate axonal conduction velocity for each hippocampal slice. For electrophysiological assessment of long-term potentiation of synaptic transmission in the medial prefrontal cortex (mPFC), modified coronal slices (Supplementary Fig. 4B) containing the prelimbic and infralimbic subregions of the mPFC were sectioned on a vibratome at 350 μm thickness (Parent *et al.*, 2010). Slices were transferred to an incubation chamber, warmed to 32°C for 30 minutes, and equilibrated in a slice recording chamber at 32°C with continuous perfusion (2 ml/min) of artificial cerebrospinal fluid (aCSF; 10 mM glucose, 126 mM NaCl, 2.5 mM KCl, 1.25 mM NaH_2PO_4, 1.3mM $MgCl_2$, 2.5 mM $CaCl_2$, 26 mM $NaHCO_3$ saturated with 95% O_2 and 5% CO_2). Synaptic transmission and long-term potentiation were assessed with a stimulating electrode placed in mixed inputs in layers V/VI and an extracellular recording electrode placed in layers II/III (Supplementary Fig. 4C).

Computational simulations

Material properties for the 4340 steel impact rod and metal (304 steel, 6061-T6 aluminum) components of the sled are given by Steinberg (Steinberg, 1996). The foam pad was modeled as a nonlinear compacting material (ISODAMP® C-1000 Series) with elastic recovery based on material properties provided by the manufacturer (EAR Specialty Composites, Indianapolis, IN). The sled, impact rod, and foam pad were modeled with 0.076 cm thick zones. Convergent solutions were validated by doubling the number of zones in the impact and blast simulations. Although higher frequencies were resolvable, the conclusions reached were unchanged. Modelling of the turbulent wake is outside the scope of this study and was modelled as a region of still air at ambient

pressure. The blue-shaded region to the right of the sphere (Fig. 7F) is maintained at ambient pressure, effectively a numerically-enforced representation of the mean properties of the turbulent wake.

Statistical analyses

Linear mixed-effects regression analyses were used to test group differences with respect to acute neurobehavioral response test scores. Linear mixed-effects regression analysis was also used to determine group differences between Evan's blue extravasation for impact and control mice as well as laterality and location by slice. For each linear mixed-effects regression analyses, we allowed for outcome specific fixed effects and subject-specific random effects. Outcomes were correlated using a single between-subject correlation by applying a compound-symmetry model for the covariance matrix. These mixed effect analyses are more realistic models of the outcome than using independent regression models for each outcome. All information within each subject was utilized, thus facilitating consistent and interpretable results without multiple comparisons (Gelman *et al.*, 2012). Multivariate models also provide greater power for detecting small but clinically important differences compared to independent regression models for each outcome (Goldstein, 2011). Immunoblot densitometry and biochemical data were evaluated by two-tailed Student's t-test. Neuroinflammation data were evaluated by one-way ANOVA followed by *post hoc* Student's t-test using Bonferroni correction. Comparisons of axonal conduction velocity and LTP magnitude between sham-control mice and impact mice 1 day, 3 days and 2 weeks post-injury were made using three-way ANOVA. Spearman's rank-order coefficient was computed between lost points on the acute neurobehavioral response test battery and TBI and CTE endpoints (Table 1). Levels of significance were indicated as follows: *, $P < 0.05$; **, $P < 0.01$; ***, $P < 0.001$; NS, not significant. Statistical significance was set at an alpha-level of $P < 0.05$. Exact P values are reported for statistical significance except when $P < 0.0001$.

Supplementary References

Baugh CM, Kiernan PT, Kroshus E, Daneshvar DH, Montenigro PH, McKee AC*, et al.* Frequency of Head-Impact–Related Outcomes by Position in NCAA Division I Collegiate Football Players. J Neurotrauma 2015; 32(5): 314-26.

Broglio SP, Sosnoff JJ, Shin S, He X, Alcaraz C, Zimmerman J. Head impacts during high school football: a biomechanical assessment. J Athletic Train 2009; 44(4): 342-9.

Chassidim Y, Veksler R, Lublinsky S, Pell GS, Friedman A, Shelef I. Quantitative imaging assessment of blood-brain barrier permeability in humans. Fluids Barriers CNS 2013; 10(9).

Chernov N. Circular and linear regression: Fitting circles and lines by least squares. Boca Raton, FL: CRC Press; 2010.

Daniel RW, Rowson S, Duma SM. Head impact exposure in youth football. Annals of biomedical engineering 2012; 40(4): 976-81.

Gelman A, Hill J, Yajima M. Why we (usually) don't have to worry about multiple comparisons. Journal of Research on Educational Effectiveness 2012; 5(2): 189-211.

Goldstein H. Multilevel statistical models. Chichester, West Sussex, UK: John Wiley & Sons, Ltd.; 2011.

Goldstein LE, Fisher AM, Tagge CA, Zhang X-L, Velisek L, Sullivan JA*, et al.* Chronic traumatic encephalopathy in blast-exposed military veterans and a blast neurotrauma mouse model. Sci Transl Med 2012; 4(134): 134ra60.

Jay TR, Miller CM, Cheng PJ, Graham LC, Bemiller S, Broihier ML*, et al.* TREM2 deficiency eliminates TREM2+ inflammatory macrophages and ameliorates pathology in Alzheimer's disease mouse models. J Exp Med 2015; 212(3): 287-95.

Kondo A, Shahpasand K, Mannix R, Qiu J, Moncaster J, Chen C-H*, et al.* Antibody against early driver of neurodegeneration cis P-tau blocks brain injury and tauopathy. Nature 2015; 523(7561): 431-6.

McKee AC, Cairns NJ, Dickson DW, Folkerth RD, Keene CD, Litvan I*, et al.* The first NINDS/NIBIB consensus meeting to define neuropathological criteria for the diagnosis of chronic traumatic encephalopathy. Acta Neuropathol 2016; 131(1): 75-86.

McKee AC, Stein TD, Nowinski CJ, Stern RA, Daneshvar DH, Alvarez VE*, et al.* The spectrum of disease in chronic traumatic encephalopathy. Brain 2013; 136(1): 43-64.

Parent MA, Wang L, Su J, Netoff T, Yuan L-L. Identification of the hippocampal input to medial prefrontal cortex in vitro. Cerebral Cortex 2010; 20(2): 393-403.

Steinberg, D. Equation of state and strength properties of selected materials. Livermore, CA USA: Lawrence Livermore National Laboratory; 1996. UCRL-MA-106439.

Taubin G. Estimation of planar curves, surfaces, and nonplanar space curves defined by implicit equations with applications to edge and range image segmentation. IEEE Transactions on Pattern Analysis & Machine Intelligence 1991(11): 1115-38.

Vonsattel JP, Aizawa H, Ge P, DiFiglia M, McKee AC, MacDonald M*, et al.* An improved approach to prepare human brains for research. J Neuropathol Exp Neurol 1995; 54(1): 42-56.

Weissberg I, Veksler R, Kamintsky L, Saar-Ashkenazy R, Milikovsky DZ, Shelef I*, et al.* Imaging blood-brain barrier dysfunction in football players. JAMA Neurol 2014; 71(11): 1453-5.

Supplementary Table 1. Human cases included in this study.

	Case	Number	Age-Sex	Sports	Post-Injury Interval	COD
Impact Head Injury Cases	Case 1	7964	18M	AF	4 months	Suicide by hanging
	Case 2	8987	18M	AF, R	10 days	Cerebral edema
	Case 3	9126	17M	AF,L	2 days	Suicide by hanging
	Case 4	7538	17M	AF	26, 6, 1 day(s)	SIS
Athlete Control Cases	Case 5	6601	19M	AF	-	Cardiac arrest
	Case 6	7134	19M	H	-	Cardiac arrhythmia
	Case 7	7176	17M	AF	-	Oxycodone overdose
	Case 8	7490	22M	AF	Remote >7 years	Suicide

AF, American football. **H**, hockey. **L**, lacrosse. **R**, rugby. **SIS**, second impact syndrome.

Supplementary Table 2A. Impact instrument operation parameters used in this study.

Impact Instrument Operation Parameters	Mean	SD	CV%	N
Fire Pressure (psig)	19.1	1.3	6.6	406
Slug Velocity (m/s)	25.4	0.7	2.8	381*
Rod Velocity (m/s)	7.2	0.3	3.9	406
Sled velocity (m/s)	5.1	0.5	9.8	406

*Excluded trials with light gate error

Supplementary Table 2B. Head kinematics in closed-head impact injury and blast exposure

Closed-Head Impact Injury Mouse Model Parameters	Impact N = 18	Blast N = 8	Statistical Significance*
Instrument Intensity Variable	Sled Velocity 5.1 ± 0.2 m/s	Peak Blast Pressure 72.3 ± 2.8 kPag	
Max Head X-Deflection (mm)	35.6 ± 2.3	34.3 ± 4.8	NS
Max Head X-Acceleration (x 10^3 m/s^2)	12.6 ± 3.4	9.0 ± 2.4	NS
Max Head Angular Acceleration ($krad/s^2$)	398.8 ± 111.0	359.0 ± 111.5	NS
Max Head X-Jerk (x 10^7 m/s^3)	5.3 ± 2.5	4.8 ± 1.1	NS
Head Swing Radius (mm)	30.0 ± 2.3	28.4 ± 3.1	NS

* NS = Not statistically different. Values represent mean ± SD.

mouse models used in this study.

Supplementary Table 2C. Impact instrument and animal subject parameters used in this study.

Animal Subject Parameters (C57BL6 ♂)	Impact		Control	
	Mean ± SD (CV%)	N	Mean ± SD (CV%)	N
Weight (g)	25.3 ± 1.8 (7.0)	203	25.3 ± 2.0 (7.9)	117
Age (weeks)	10.2 ± 0.7 (6.7)	203	10.1 ± 0.4 (4.5)	117

Supplementary Table 3. Composite scores on acute neurobehavioral response test battery do not correlate with TBI-CTE endpoints in the acute-subacute period after experimental closed-head impact injury in mice.[1]

BBB Disruption[2†]	$CD45^+$ Monocyte CNS Infiltration[3†]	Phospho-Tau Proteinopathy[4†]	Slowed Axonal Conduction (HIPP)[5†]	Defective Synaptic LTP (mPFC)[6†]
24 hours[†]	3 days[†]	2 weeks[†]	24 hours, 3 days, 2 weeks[†]	+24 hours, 3 days, 2 weeks[†]
Spearman	Spearman	Spearman	Mixed Model	Mixed Model
$\rho = 0.29$	$\rho = -0.09$	$\rho = -0.50$	$F = 0.86$	$F = 2.32$
p = 0.36	p = 0.86	p = 0.20	p = 0.53	p = 0.15
NS	NS	NS	NS	NS

† Time points represent maximal post-injury response for each index metric.
[1] Acute neurobehavioral response test battery, composite score after impact.
[2] BBB disruption by quantitative Evans blue fluorescence imaging.
[3] CD45+ inflammatory cells in the brain by flow cytometry.
[4] Phosphorylated tau protein by quantitative immunoblotting.
[5] Hippocampal axonal conduction velocity, CA1 subregion.
[6] LTP in the medial prefrontal cortex (mPFC, prelimbic region).
[7] NS = correlation is not statistically significant.

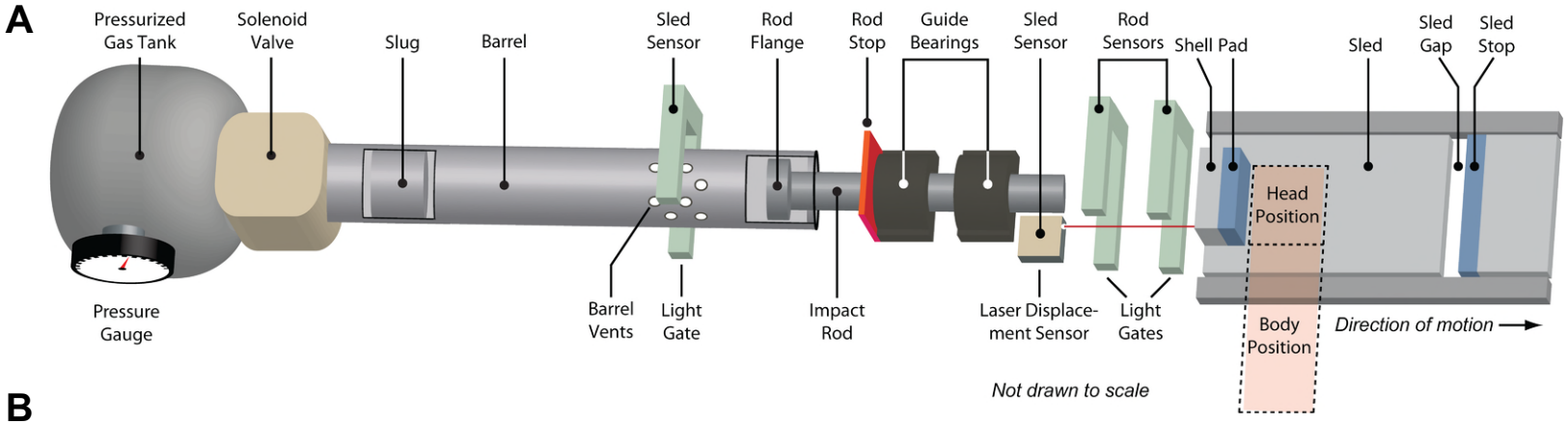

B

Subtest 1 OpenField* (30 secs)	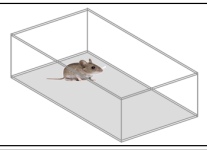	**Score = 5** A Linear locomotion B Explores 2 or more corners	**Score = 4** A Linear locomotion B Explores <2 corners	**Score = 3** A Unidirectional rotation B Note rotation direction	**Score = 2** A No locomotion B Ventral abdomen down	**Score = 1** A No locomotion B Lateral abdomen down	**Score = 0** A Tonic-Clonic Seizure B Note unilateral or general	**1** Open Field Sub-Score
Subtest 2 Inverted Wire Mesh* (30 secs)	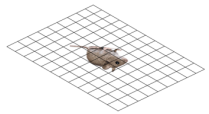	**Score = 5** A Multidirectional locomotion, *Paw exits box at least once* B Four-paw hang	**Score = 4** A Multidirectional locomotion, *Paws remain within box* B Four-paw hang	**Score = 3** A Unidirectional rotation* B Four-paw hang **Note direction of rotation*	**Score = 2** A No Locomotion B Four-paw hang	**Score = 1** A No Locomotion B <Four-paw hang	**Score = 0** A Unable to grip mesh *or* B Falls from mesh	**2** Wire Mesh Sub-Score
Subtest 3 Beam Walk* (30 secs)		**Score = 5** A Beam traversal B Total distance ≥ ½ beam	**Score = 4** A Beam traversal B Total distance < ½, ≥ ¼ beam	**Score = 3** A Beam traversal B Total distance < ¼ beam	**Score = 2** A No beam traversal B Balances on beam	**Score = 1** A No beam traversal B Unbalanced on beam	**Score = 0** A Unable to perform test *or* B Falls from beam	**3** Beam Walk Sub-Score

*Validated only for anesthesia-naïve C57BL/6 male mice. Note: "A" Criteria: dominant mode of locomotion. "B" Criteria: criterion modifier. Rate subdomain criteria to highest score.

Composite Test Battery Score

Supplementary Fig. 1. Impact instrument and acute neurobehavioral response test battery. A) Schematic of the impact instrument used in this study. The instrument utilizes a pressurized gas-driven momentum transfer mechanism to deliver a non-skull-deforming closed-head impact injury. B) Acute neurobehavioral response scale test battery for ***awake, non-anesthetized (anesthesia-naïve) mice***. Impact-injured mice demonstrated a constellation of post-traumatic deficits across multiple neurobehavioral domains (arousal, responsivity, locomotion, exploration, habituation, motor performance) with abrupt onset, transient course, rapid recovery, and complete resolution of deficits. *The observed deficits, time course, and recovery resemble acute concussion in humans* (Supplementary Video 1). The test battery comprises three subtests: open field, inverted wire mesh, and beam walk. Acute responses to experimental head injury are captured on a 16-point scale (0–15; composite score, sum of subtest scores). A maximum composite score of 15 indicates unimpaired performance, whereas a composite score of 0 indicates severe impairment. Each subtest is conducted over 30 seconds, video recorded, and graded by an observer blind to treatment status on a 6-point scale (0–5) according to observable metrics that capture graded, multidimensional impairment specific to each subtest. The complete test battery (three subtests) is conducted *before* experimental injury (pre-injury), *after* experimental injury (post-injury), and *after* a 3-hour rest period (recovery).

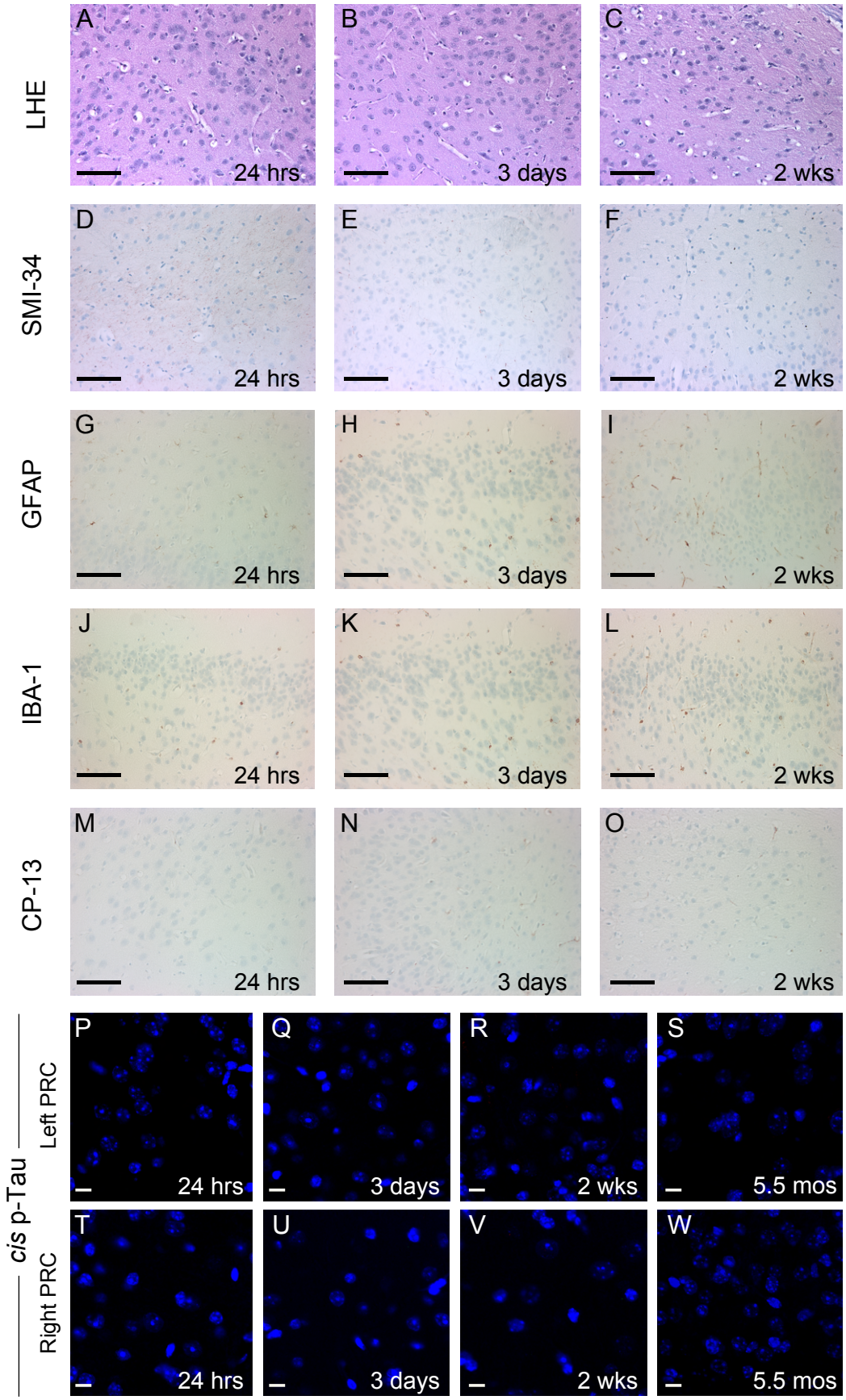

Supplementary Fig. 2. (A–O) Absence of neuropathology in the left perirhinal cortex of mice exposed to the sham (no injury) control condition. (P–W) *Cis*-p-tau brain pathology was not observed in the perihinal cortex of either hemisphere after sham (no injury) control exposure. Markers and time points as indicated. Scale bars (Panels A–O), 100 µm. Scale bars (Panels P–W), 20 µm.

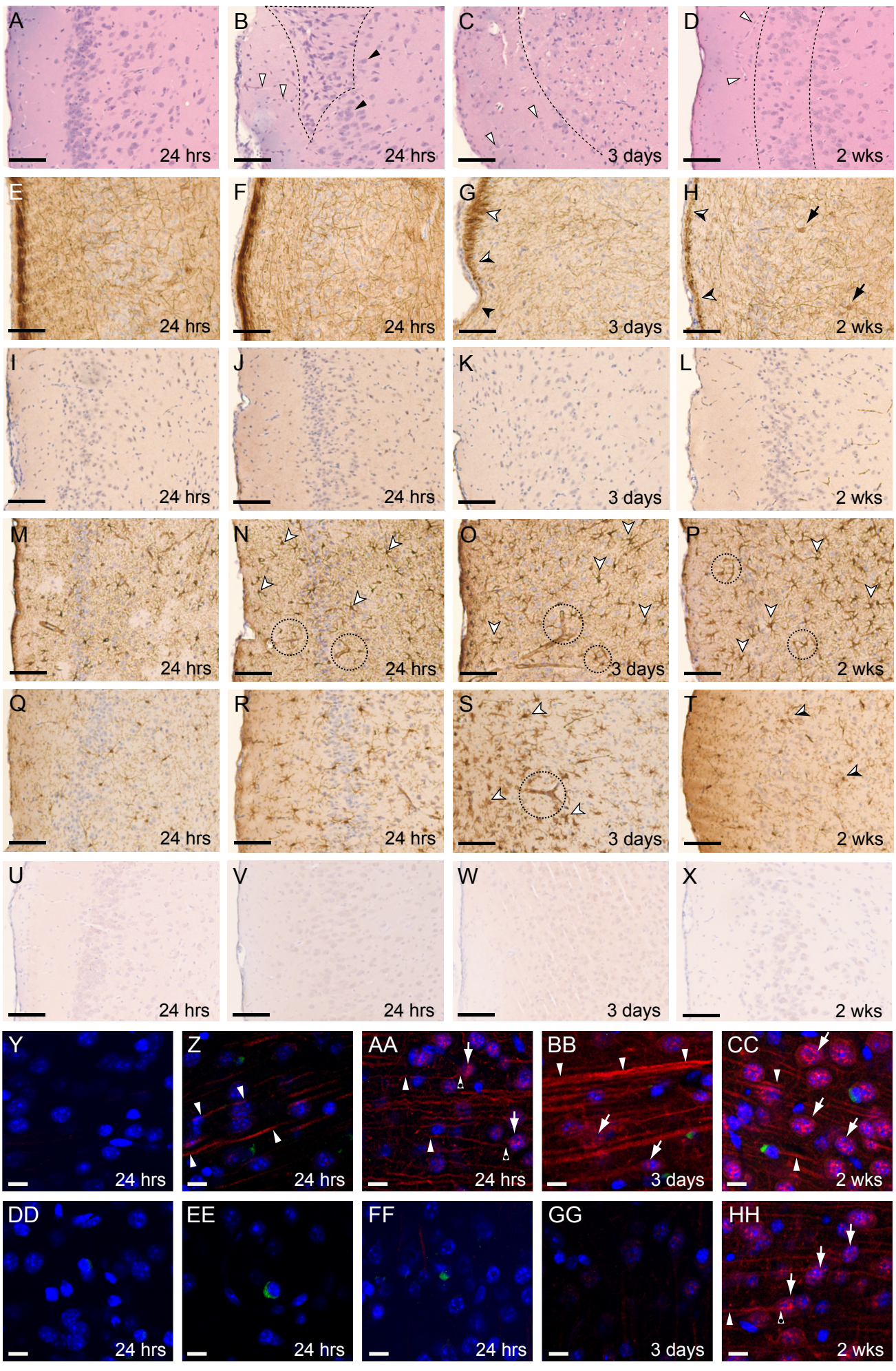
Right PRC
Left PRC
LHE
SMI-34
APP/Aβ
GFAP
IBA-1
CP-13
cis-p-tau
Left PRC
Right PRC
A
B
C
D
E
F
G
H
I
J
K
L
M
N
O
P
Q
R
S
T
U
V
W
X
Y
Z
AA
BB
CC
DD
EE
FF
GG
HH
24 hrs
3 days
2 wks

Supplementary Fig. 3. Experimental exposure to a single closed-head impact injury induces traumatic microvascular injury, astrocytosis, microgliosis and progressive phosphorylated tauopathy) in cerebral cortex ipsilateral and subjacent to the impact contact zone. Brain pathologies and time course are similar to results obtained in mice subjected to two closed-head impact injuries with a separation interval of 15 minutes (Fig. 3). (A–D) Luxol fast blue hematoxylin and eosin (LHE) staining in the unaffected contralateral (right) perirhinal cortex (PRC; A) and injured ipsilateral (left) PRC at 24 hours (B), 3 days (C), 2 weeks (D) after exposure to a single impact injury. (A) Cytoarchitecture in the unaffected contralateral PRC 24 hours after injury is normal and neuropathologically indistinguishable from the corresponding PRC in uninjured sham control mice sacrificed at the same time point. Scale bar, 100 μm. (B,C) LHE staining in the injured ipsilateral (left) PRC at 24 hours (B) and 3 days (C) post-injury revealed large cortical areas of dying neurons (black hashed line) with pyknotic basophilic nuclei and faintly eosinophilic cytoplasm. At 24 hrs post-injury (B), numerous normal-appearing neurons (black arrowheads) were present. By 3 days post-injury (C), the injured cortex showed marked diminution in neuronal density (right side of hashed line) and evidence of parenchymal rarefaction consistent with neuronal demise. Small penetrating blood vessels (white arrowheads) are present (B,C). Scale bars, 100 μm. (D) By 2-weeks post-injury, the injured cortex shows signs of tissue recovery. Decreased neuronal density is evident in the cortical region between the black hashed line. A small penetrating blood vessel (white arrowheads) is present. Note: the contralateral (right) PRC was histopathologically normal by LHE staining (A) at all time points and was indistinguishable from the unaffected left and right PRC in uninjured sham control mice. Scale bar, 100 μm. (E–H) Immunostaining with monoclonal antibody SMI-34 (phosphorylated neurofilament) in the unaffected contralateral (right) PRC (E) and injured ipsilateral (left) PRC at 24 hours (F), 3 days (G), and 2 weeks (H) after exposure to a single impact injury. Focal loss of SMI-34 immunoreactivity was evident to varying degree (arrowheads, black > black-white > white) by 3 days (G) and to a greater spatial extent by 2 weeks (H) post-injury. Abnormal accumulation of SMI-34 immunoreactivity (black arrows) was observed at the later time point (H). Note: the contralateral (right) PRC was histopathologically normal by SMI-34 immunostaining at all time points. Scale bars, 100 μm. (I–L) Immunostaining with monoclonal antibody 4G8 (APP, amyloid precursor protein; amyloid-β peptide, Aβ) was not detected in the unaffected contralateral (right) PRC (I) or in the injured ipsilateral (left) PRC at 24 hours (F), 3 days (G), or 2 weeks (H) after exposure to a single impact injury. Note: the contralateral (right) PRC was histopathologically normal by APP/Aβ immunostaining at all time points. Scale bars, 100 μm. (M–P) Immunostaining for glial fibrillary acidic protein (GFAP) in the unaffected contralateral (right) PRC (M) and injured ipsilateral (left) PRC at 24 hours (N), 3 days (O), and 2 weeks (P) after exposure to a single impact injury. (M) Normal field of non-reactive astrocytes were present in the unaffected contralateral (right) PRC 24 hours post-injury. (N) Modest astrocytosis was evident 24 hours post-injury. Reactive perivascular astrocytes with large endfeet were evident at this time point (black hashed circles). (O,P) Brisk reactive astrocytosis at 72 hours post-injury (O) and resolving astrocytosis at 2 weeks post-injury (P). Clusters of hypertrophied GFAP-immunopositive reactive astrocytes (white arrowheads) with extensively ramified processes and perivascular astrocytes (arrow) with hydropic end-feet terminating on small blood vessels (hashed circles) were present at this time point. Note overlapping astrocytic processes indicative of disrupted domain restriction. Note: the contralateral (right) PRC was histopathologically normal by GFAP immunostaining at all time points. Scale bars, 100 μm. (Q–T) Immunostaining for the myeloid cell marker Iba1 in the unaffected contralateral (right) PRC (Q) and injured ipsilateral (left) PRC at 24 hours (R), 3 days (S), and 2 weeks (T) after exposure to a single impact injury. (Q) Normal field of non-reactive microglia were present in the unaffected contralateral (right) PRC 24 hours post-injury. (R,S) Evidence of microglal reactivity at 24 hours post-injury (R) and peak microgliosis at 3 days post-injury (S). Clusters of intensely Iba1-immunoreactive, highly-ramified myeloid cells (white arrowheads, S) and less abundant ameboid and rodlike Iba1-immunoreactive microglia were observed at both time points. Iba1-immunoreactive perivascular myeloid cells were often associated with the parenchymal (abluminal) surface of a small blood vessel (hashed circle, S). (T) Microgliosis was largely resolved by 2 weeks post-injury. A few residual clusters of activated microglia with overlapping processes were evident at this time point. Note: the contralateral (right) PRC was histopathologically normal by Iba1 immunostaining at all time points. Scale bars, 100 μm. (U–X) Immunostaining for phosphorylated tau protein with monoclonal antibody CP13 (pS202) was not detected in the unaffected contralateral (right) PRC (U) or in the injured ipsilateral (left) PRC at 24 hours (V), 3 days (W), or 2 weeks (X) after exposure to a single impact injury. Note: the contralateral (right) PRC was histopathologically normal by CP13 immunostaining at all time points. Scale bars, 100 μm. (Y–HH) Immunohistofluorescence staining for cis-p-tau protein (cis-motif, pThr231-Pro), a highly pathogenic early phosphorylated tau proteoform, in the injured ipsilateral (left) PRC at 24 hours (Y,Z,AA), 3 days (BB), and 2 weeks (CC) and in the unaffected contralateral (right) PRC at 24 hours (Y,Z,AA), 3 days (BB), and 2 weeks (CC) after exposure to a single impact injury. Faint cis-p-tau immunoreactivity was observed in axons (arrowheads) in the left PRC in some mice (Z,AA) but not others (Y) 24 hours post-injury. Aberrant somatodendritic cis-p-tau accumulation with dot-like inclusions (arrows) were also observed at this time point. The unaffected contralateral (right) PRC (DD,EE,FF) was uniformly nonreactive for cis-p-tau. Green immunohistofluorescence (EE), trans-p-tau. Scale bars, 20 μm. By 3 days post-injury, cis-p-tau immunoreactivity in the ipsilateral perirhinal cortex (BB) was intense, not only in axons (arrowheads), but also as dot-like inclusions in neuronal soma and dendrites (arrows). Cis-p-tau immunoreactivity

was not detected in the contralateral perirhinal cortex (FF) at this time point. Green immunohistofluorescence (EE), trans-p-tau. Scale bars, 20 μm. By 2 weeks post-injury, cis-p-tau immunoreactivity was observed in axons (arrowheads) and as dot-like inclusions in neuronal soma and dendrites (arrows) in both hemispheres (left PRC, CC; right PRC, HH). While cis-p-tau immunoreactivity was evident in both hemispheres, this pathology was more pronounced in the ipsilateral PRC (left, CC) than in the contralateral PRC (right, HH). Sham (no-injury) control mice did not show evidence of cis-p-tau immunoreactivity in either hemisphere at any of the analyzed time points. Scale bars, 20 μm.

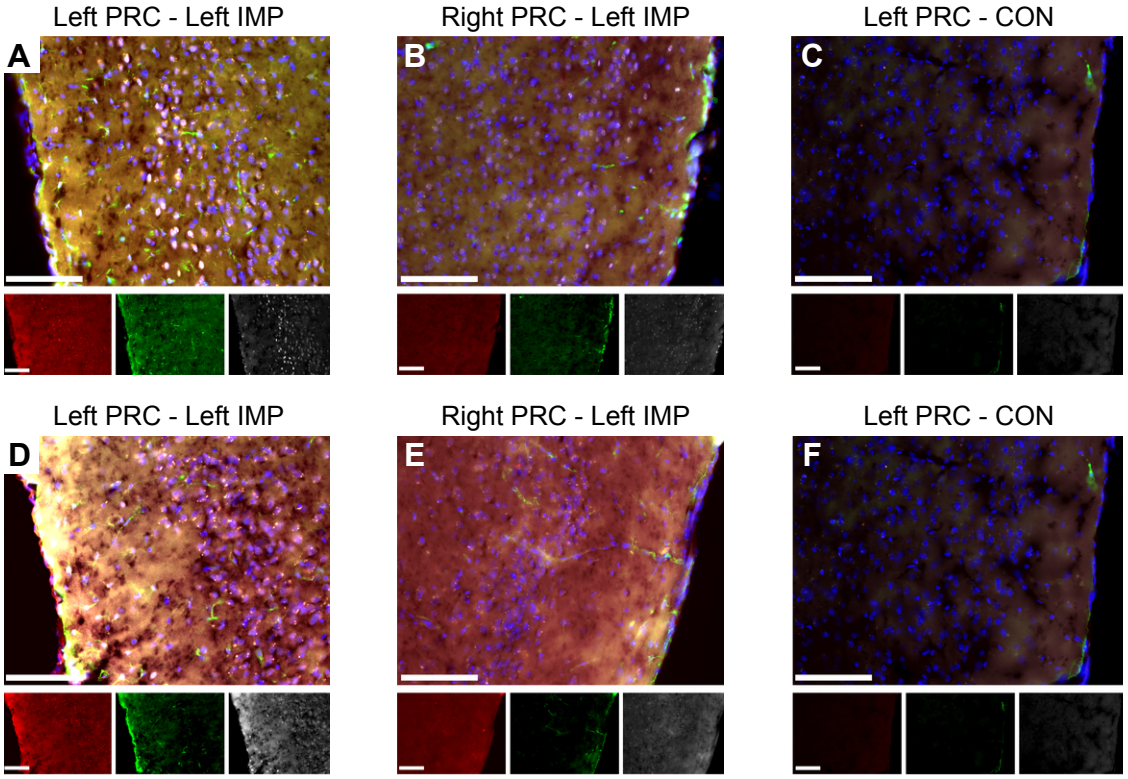

Supplementary Fig. 4. (A–F) Colocalization of extravasated serum albumin (SALB), astrocytic glial fibrillary acidic protein (GFAP), phosphorylated-SMAD2 (pSMAD2), and transforming growth factor-β (TGFβ) in the ipsilateral but not contralateral perirhinal cortex (PRC) 3 days after exposure to unilateral (left-side) closed-head impact injury (IMP) or sham (no injury) control (CON). (A) Ipsilateral (left) perirhinal cortex, IMP. (B) Contralateral (right) perirhinal cortex, IMP. (C) Ipsilateral (left) perirhinal cortex, CON. (A–C) p-Smad2 (gray), SALB (red), GFAP (green), DAPI (blue). (D) Ipsilateral (left) perirhinal cortex, IMP. (E) Contralateral (right) perirhinal cortex, IMP. (F) Ipsilateral (left) perirhinal cortex, CON. (D–F) TGF-β (gray), SALB (red), GFAP (green), DAPI (blue). Split color channel photomicrographs are shown below larger composite photomicrographs. Magnification (larger composite images), 20X. Scale bars, 100 µm.

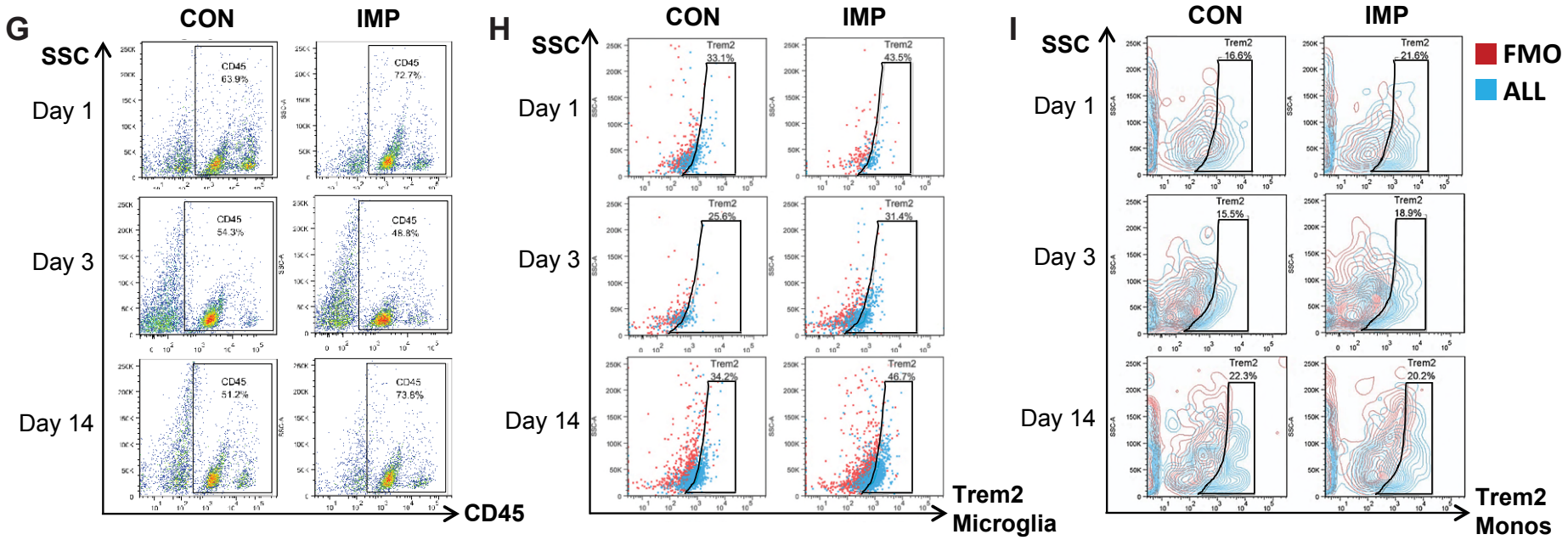

(G–I) Flow cytometry results from mouse brains 1 day, 3 days, 2 weeks after closed-head impact injury (IMP) or sham (no-injury) control condition (CON). (G) $CD45^{+}$inflammatory cells. (H) Trem2+ microglia ($TREM2^{+}CD45^{low}CD11b^{+}$). (I) Trem2+ monocytes ($CD45^{high}CD11b^{+}Ly\text{-}6G^{-}$).

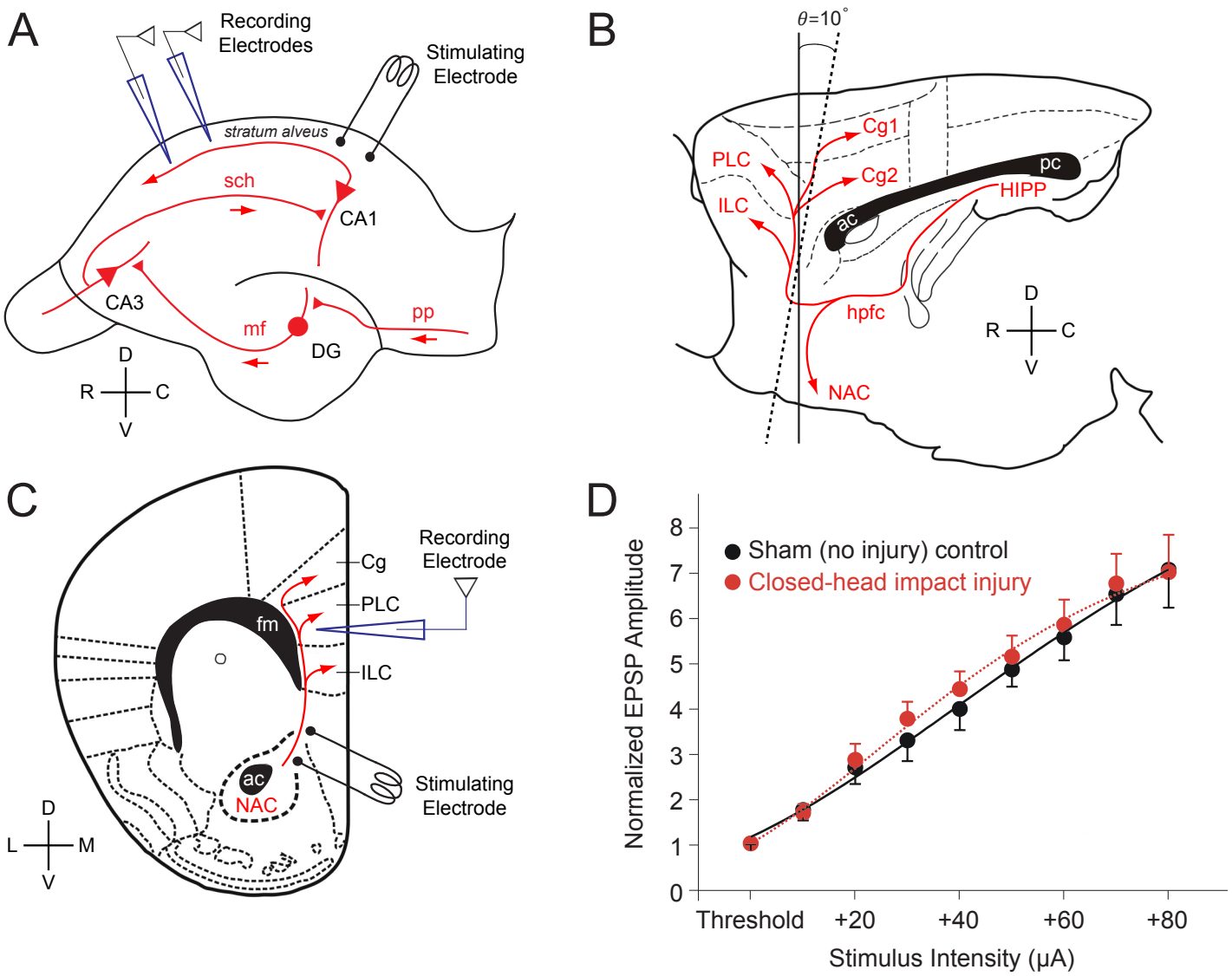

Supplementary Fig. 5. Hippocampal and medial prefrontal cortical neuroanatomy in relationship to electrophysiology slice preparation. (A) Electrophysiological arrangement for evaluation of hippocampal axonal conduction velocity. CA1, CA3: hippocampus regions (cornu Ammonis 1,3); dg, dentate gyrus; mf, mossy fiber pathway; pp, perforating pathway; sch, Shaffer collateral pathway. D, V, R, C: dorsal, ventral, rostral caudal. Stimulating and recording electrodes as shown. (B) Sagittal section of mouse brain showing medial prefrontal cortex (mPFC) and connections with the hippocampus. ac, anterior commissure; cg1,2, cingulate cortex regions 1,2; hipp, hippocampus; hpfc, hippocampal-prefrontal cortical pathway; ilc, infralimbic subregion of mPFC; nac, nucleus accumbens; pc, posterior commissure; plc, prelimbic subregion, mPFC. D, V, R, C: dorsal, ventral, rostral caudal. (C) Electrophysiological arrangement for evaluation of long-term potentiation (LTP) of synaptic neurotransmission in mPFC. ac, anterior commissure; cg, cingulate cortex; fm, forceps minor; ilc, infralimbic subregion, mPFC; NAC, nucleus accumbens; plc, prelimbic subregion, mPFC. D, V, L, M: dorsal, ventral, lateral, medial. Stimulating and recording electrodes as shown. (D) Post-impact injury white matter-evoked synaptic field potential input-output relations.

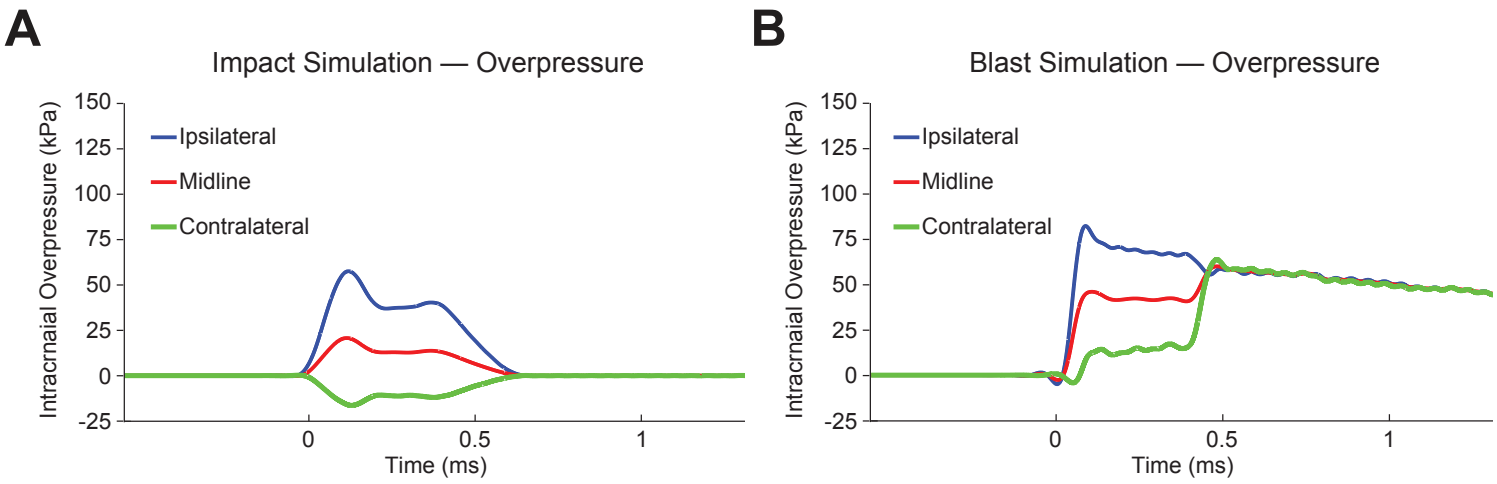

Supplementary Fig. 6. Intracranial overpressure curves generated in response to impact (A) or blast (B) simulations at three Lagrangian tracer locations in the model mouse brain. Markers (i, blue; m, red; c, green) correspond to ipsilateral, medial, and contralateral locations, respectively, in the model mouse brain as noted in Fig. 7E, F. (A–B) Peak overpressure at the ipsilateral (i) tracers are comparable in response to impact and blast simulations. In both simulations, pressure gradients at the ipsilateral, medial, and contralateral tracers resolve within 0.75 ms. The decaying residual overpressure in the blast simulation correresponds to the decaying extracranial overpressure produced by the blast shock wave.